P2.24 WATER VAPOR TRANSPORT OVER THE PACIFIC OCEAN DURING EL NIÑO AND LA NIÑA: A SATELLITE APPROACH

B.J. Sohn[1], Seong-Chan Park[1], Franklin R. Robertson[2], and Eric A. Smith[3]

[1]School of Earth and Environmental Sciences
Seoul National University, Seoul, Korea
E-mail: sohn@snu.ac.kr

[2]Global Hydrology and Climate Center (GHCC), NASA/MSFC
Huntsville, AL

[2]NASA Goddard Space Flight Center
Greenbelt, MD

1. INTRODUCTION

One of important problems of the atmospheric water budget is the role of water vapor transport in atmospheric circulation whose convergence provides, in part, spatial distribution of heating due to the latent heat release. Considering that spatial distribution of the heating is a main forcing driving the atmospheric circulation over the tropics, the examination of water vapor transport would bring in better understanding of atmospheric circulation. However, little attention is given to what extent of mean or extreme climate is contributed by water vapor transport or vice versa, in particular, associated with long term widespread droughts or floods.

Recent advent of PMW measurements from space such as Special Sensors for Microwave Imager (SSM/I) on board DMSP satellite and TMI on board TRMM satellite provides atmospheric water budget parameters, i.e., water vapor, cloud liquid water, and precipitation to investigate water budget within the atmosphere. Satellites also offer global spatial coverage with consistent quality and high temporal sampling which lead to an improved estimation of latent heat flux and to an improved climatology with remote sensing techniques (Chou et al., 1995; Schulz et al., 1997).

Thus, it is now possible to carry out a purely satellite-based water budget over the global oceans, which in essence, captures all of the important water budget components and transport features. In this study, we will construct atmospheric branch of hydrologic cycle by combining estimates of precipitation and evaporation from recent spaceborne sensors, without requiring information on the wind and moisture profiles over the globe.

*Corresponding Author's Address: Dr. B.J. Sohn
School of Earth and Environmetal Sciences
Seoul National University, Seoul, 151-742, Korea.
E-mail: sohn@snu.ac.kr

2. BACKGROUND AND METHODOLOGY

The balance equation for the vertically integrated total water in an atmospheric column can be expressed by:

$$\frac{\partial(W + W_C)}{\partial t} + div(Q + Q_C) = E - P \qquad (1)$$

where $W+W_c$ and $Q+Q_c$ are the column integrated total water and horizontal water transport vector, respectively. Often, transports related to condensation terms are small, thus, eq (1) is simplified over specified time and space domains:

$$[\frac{\partial(W + W_c)}{\partial t}] + [divQ] = [E - P] \qquad (2)$$

Traditionally, large-scale water vapor transport [Q] has been derived directly from circulation statistics in which transport processes are often depicted by mean and eddy motions (Peixoto and Oort, 1992). Detailed and accurate calculations of three-dimensional moisture transport terms over the globe are required. Notably, the lack of systematically spaced conventional measurements of meteorological variables over oceans has hindered understanding of the distribution and transport of water vapor. This motivates the use of indirect calculation methods. Assuming the rate of changes of precipitable water and condensates is small over a sufficiently long time period, horizontal divergence of water vapor is balanced by the evaporation minus precipitation, [E-P], i.e.:

$$divQ = [E-P] \qquad (3)$$

Introducing water vapor transport potential function (F) and separating water vapor transport into rotational (Q_R) and divergent (Q_D) components, we can solve water vapor transport, i.e.:

$$divQ = [E-P] = \tilde{N}^2 F \qquad (4)$$

$$[Q_D] = -\tilde{N} F \qquad (5)$$

Eqs. (4) and (5) are solved on a complete global domain using the spectral method. The divergent

component of water vapor transport then will be examined in conjunction with tropical circulation changes associated with SST variations during El Niño and La Niña periods.

3. Data Sets

For solving Eqs. (4) and (5), we need [E-P] information. Precipitation data for seven year (1988-94) mean climatology are derived from SSM/I measurements. But, for the transport calculation of El Nino and La Nina periods, we use precipitation data from combination of different data sources, i.e., monthly average unclipped TRMM Microwave Imager (TMI) estimate, monthly SSM/I, pentad geostationary infrared (IR) estimates, and the monthly accumulated Climate Assessment and Monitoring System (CAMS) or Global Precipitation Climatology Centre (GPCC) rain gauge analysis. They are obtained from NASA GSFC data distribution center.

The evaporation (E) is estimated from the bulk aerodynamic method, i.e.:

$$E = \rho C_E(U-U_s)(q_s-q) \quad (6)$$

where ρ is air density, C_E is bulk transfer coefficient, U is the wind speed at the reference height and U_s is the ocean surface current, and q and q_s are specific humidity at the reference height and ocean surface, respectively. We used Chou's algorithm (Chou et al., 1995) with inputs of SST, specific humidity and wind speed at 10 m above the sea surface, air temperature at 2 m above the surface. In this study, 10 m wind speed is derived from SSM/I products (Wentz, 1992). Humidity at the surface layer is also estimated from SSM/I measurements by applying the relationship of surface humidity - lowest 500 m boundary layer water vapor (Schulz et al., 1993).

Since the SSM/I-derived evaporation is only available over oceans, boundary conditions along the continental outline are required for solving Eq. (5). Instead of specifying boundary conditions NCEP data provide [E-P] distributions over the land so that potential function in Eq. (5) can be solved in the entire global domain.

4. Seven Year (1988-94) Mean Atmospheric Moisture Transport

a. Satellite-derived Atmospheric Moisture Transport

Satellite-derived seven year January, February, March (JFM) mean P, E, and Q_D with Φ and divQ_D are displayed in Fig. 1a-c, respectively. Prominent features found in the precipitation map (Fig. 1a) include local maxima over the intertropical convergence zone (ITCZ) north of equator over the eastern Pacific, and western Pacific maritime continent and southeastern Asia, and over the South Pacific convergence zone (SPCZ). Also noted is a precipitation zone over the northern hemispheric storm tracks over the midlatitudes of the North Pacific and Atlantic Ocean.

Seven year JFM mean evaporation was estimated from SSM/I brightness temperature measurements using Chou (1993) retrieval algorithm -- Fig. 1b. The maximum evaporation rates are found over the North Pacific off the East Asian continent and over the east coast off North America. They are due to dry and cold air advection from the continent eastward onto the warm oceans during the winter period. Evaporation rates larger than 6 mm/day are also found in the subtropical trade wind zones over the North Pacific and Atlantic Ocean. In the Southern Hemispheric oceans, it is found that the more zonal distribution with relatively large values over the subtropical latitudes. Spatial variations of E are much smaller than those of P, indicating that spatial distributions of fresh water flux (E-P) are mainly controlled by precipitation.

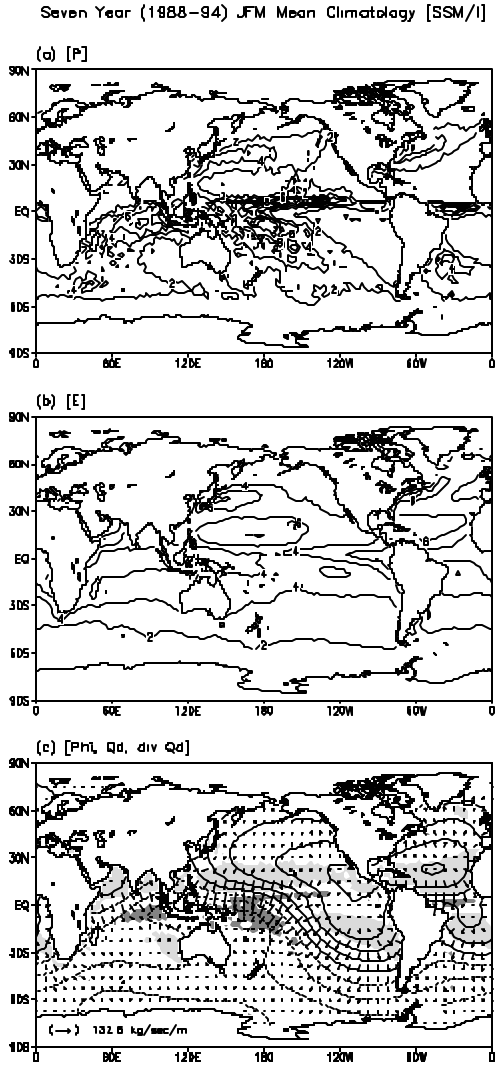

Fig. 1: Satellite-derived seven year JFM mean (a) precipitation [P], (b) evaporation [E], and (c) the resultant divergent component of water vapor transport [Q_D] with its potential function [Φ], and flux divergence [div Q_D]

The resultant divergent component of water vapor transport (Q_D) is illustrated in Fig. 1c, with its potential function [Φ], and divergence [div Q_D]. The transport vector field shows southward transport over most of oceans except north of 30°N, with a maximum at 10°N. Due to the cross-equatorial moisture flux and weak northward transport over the North Pacific and North Atlantic, the northern hemispheric subtropical oceans form moisture source regions, in which evaporated moistures are carried onto deep moisture sink convective regions by the lower tropospheric branch of the Hadley circulation.

b. NCEP-evaluated Atmospheric Moisture Transport

Seven year mean climatology is also obtained from NCEP reanalysis data (results are not shown). Compared to SSM/I estimates, large-scale features agree well but differences are significant over some areas. In the ITCZ, magnitudes are smaller and heavy rain areas (>6mm/day) are broader. Similar behaviors are found over the SPCZ region. In comparison to weak precipitation within the subtropical high, NCEP precipitation field shows stronger rain rate, especially over the eastern Pacific of the Southern Hemisphere. Heavier rain rates are also found in the midlatitude storm tracks of the Northern Hemisphere.

NCEP evaporation also shows good agreement with SSM/I estimates, e.g., a minimum in the cold tongue over the equatorial eastern Pacific, high evaporation features over the subtropical oceans and over the North Pacific and the North Atlantic off the continents. However, differences in magnitude are noticeable over the subtropical North Pacific and the southeastern Pacific off the Peruvian coast.

Moisture transport vector field derived from NCEP E-P field shows similar patterns to that found in the SSM/I derived transport vector field.

c. Zonal and Meridional Mean Transport

Mean meridional moisture transports from SSM/I and NCEP analyses, averaged only over oceans, are given in Fig. 2. It is evident that predominant southward transports occur throughout the tropics and the Southern Hemisphere, with a maximum of 67 kg s^{-1} m^{-1} for SSM/I and 51 kg s^{-1} m^{-1} for NCEP at about 10°N, leading to net water vapor flux into the Southern Hemisphere during the January to March season. It is of interest to note that there is a local minimum of southward transport (or poleward transport) around 15°S latitude. This is due to slight equatorward transport over the Indian Ocean and the southwestern Pacific off Australian continent around 15°S, which then contributes moisture flux convergence over the equatorial western Pacific and Indian Ocean. Thus, the deficit of moisture (precipitation excess) between 10°N and 10°S is compensated by the moisture convergence due to dominant southward transport associated with returning low branch of the Hadley circulation.

The corresponding east-west moisture transport, averaged over the equatorial belt from 10°N to 10°S, is displayed Fig. 3. Most of the equatorial Pacific west of about 110°W shows westward transport with a maximum of 45 kg s^{-1} m^{-1} around 160°W whose magnitude is comparable to north-south component. Distributions of east-west transport result in moisture divergence between 110°W and 160°W and convergence over the western Pacific, consistent with expected from the east-west Walker circulation.

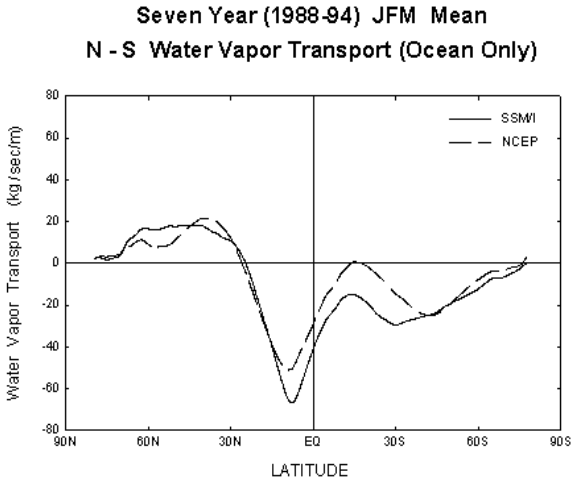

Fig. 2: Mean meridional moisture transports from SSM/I and NCEP reanalyses, averaged only over oceans.

5. Interannual Variability of Moisture Transport

In order to investigate the behavirors of water vapor transport during El Nino and La Nina we first examine SST variations during the ENSO period (not shown) from the seven year (1988-94) JFM mean SST climatology. The anomalous SST for JFM 1998 is similar to that found in typical ENSO SST anomalies, showing positive anomalies with maximum up to 3°C over most of equatorial central-eastern Pacific and a negative anomalies surrounding the positive anomaly area, with a horse-shoe shape over the western Pacific and the adjacent subtropics in both hemispheres. Sharp contrasts are noticed during the La Nina period. Most of the tropical central to eastern Pacific shows negative anomalies, in which the maximum up to -2°C is located near the dateline, representing the reestablishment of the tongue of cold surface water over the eastern Pacific.

Precipitation, evaporation, and associated moisture transport for JFM 1998 are obtained for the prevailed El Nino event. The precipitation pattern shows increased rainfall over the central Pacific, especially west of the maximum SST anomaly, with large reduction in rainfall in the South Pacific convergence zone and in the tropical western Pacific.

Compared to seven year mean climatology, the

distribution evaporation shows substantially increased moisture flux over subtropical oceans, especially in the North Pacific. Taken together, stronger Hadley-type circulation connecting more vigorous upward motion in the equatorial region to more intensified sinking motion over the North Pacific is expected.

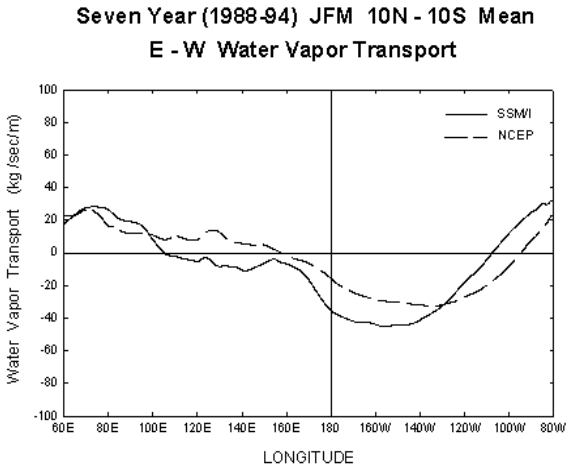

Fig. 3 The east-west moisture transports from SSM/I and NCEP reanalyses, averaged over the equatorial belt from 10°N to 10°S.

The corresponding water vapor transport field reveals that there exist a dominant east-west coupled water vapor transport, in which moisture is transported from the eastern Pacific into the western Pacific warm pool region, associated with the enhanced Walker circulation during the La Niña. But transport magnitude appears to be smaller, compared to that exited during the El Nino.

Moisture transport anomalies from seven year mean climatology with potential function and transport-induced flux convergence anomalies are given in Fig. 4. Results indicate that there are distinct differences in water vapor transport anomalies between the El Niño and the La Niña. During the El Niño period, anomalous vapor transports whose magnitudes are comparable to found in the mean field take places in the eastern half of the tropical Pacific, with strong eastward vapor transport from the date line to the equatorial eastern Pacific and equatorward transport from the subtropics of both hemispheres.

Although the general circulation of the atmosphere is driven by differential heating due to radiation energy and heat transfer from surface, orography and rotational effect, it is relatively simple to understand the time-averaged flow in the tropics because of the thermally direct circulation (Gill, 1980). There are number of studies modeling the circulation over the tropics in particular, in response to SST changes. Lindzen and Nigam (1987) showed that the boundary layer flow is much tied to the SST gradient, with an incorporation with deep convection. Modeling the moist stability diagnosed on the basis on SST, a number of studies successfully explained the position of circulation as an SST-driven phenomenon with low-level convergence and convection over warmer area (Held, 1982; Neelin and Held, 1987). Moisture transport generated by the dynamical response to the SST anomalous forcing and interactions with circulation tend to enhance the transport, maintaining a more vigourous hydrological cycle associated with enhance and Walker circulations.

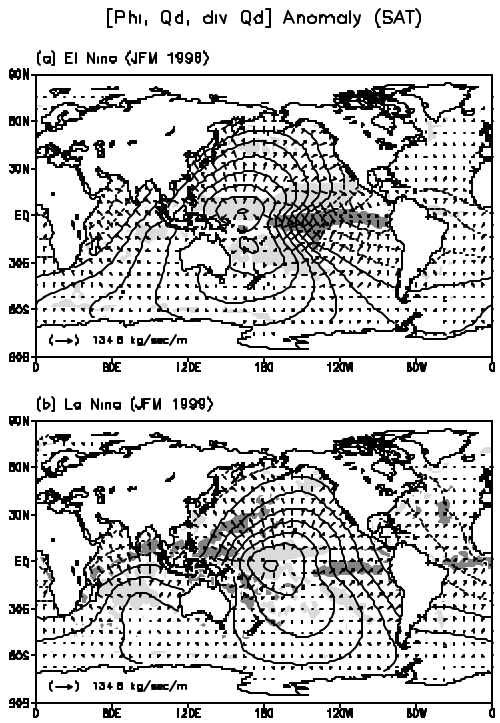

Fig. 4: Water vapor transport anomalies for (a) El Nino and (b) La Nina.

Acknowledgement

This reaseach has been supported by Minisitry of Science and Technology of Korea [Grant number: I-00-007]

References

Chou, S.-H., R.M. Atlas, C.-L. Shie, and J. Ardizzone, 1995: Estimates of surface humidity and latent heat fluxes over oceans from SSM/I data. *Mon. Wea. Rev.*, **123**, 2405-2425.

Gill, A.E., 1980: Some simple solutions for heat-induced tropical circulation. *Quart. J. Roy. Meteor. Soc*., **106**, 447-462.

Lindzen, R.S., and S. Nigam, 1987: On the role of surface sea surface temperature gradients in forcing low-level winds and convergence in the Tropics. *J. Atmos. Sci*., **44**, 2418-2435.

Peixoto, J.P., and A.H. Oort, 1992: *Physics of Climate.* American Institute of Physics, New York, 520 pp.

Schulz, J., J.M. Meywerk, S. Ewald, and P. Schluessel, 1997: Evaluation of satellite-derived latent heat fluxes. *J. Clim*., **10**, 2782-2795.